

# Walk-off Controlled Self-Starting Frequency Combs in $\chi^{(2)}$ Optical Microresonators

S. Smirnov<sup>1</sup>, B. Sturman<sup>2</sup>, E. Podivilov<sup>1,2</sup>, and I. Breunig<sup>3,4</sup>

<sup>1</sup>*Novosibirsk State University, 630090, Novosibirsk, Russia*

<sup>2</sup>*Institute of Automation and Electrometry, Russian Academy of Sciences, 630090 Novosibirsk, Russia*

<sup>3</sup>*University of Freiburg, Department of Microsystems Engineering - IMTEK, Georges-Köhler-Allee 102, 79110 Freiburg, Germany*

<sup>4</sup>*Fraunhofer Institute for Physical Measurement Techniques, 79110 Freiburg, Germany*

(Dated: March 4, 2022)

Investigations of frequency combs in  $\chi^{(3)}$  optical microresonators are burgeoning nowadays. Changeover to  $\chi^{(2)}$  resonators promises further advances and brings new challenges. Here, the comb generation entails not only coupled first and second harmonics (FHs and SHs) and two dispersion coefficients, but also a substantial difference in the group velocities – the spatial walk-off. We predict walk-off controlled highly stable comb generation, drastically different from that known in the  $\chi^{(3)}$  case. This includes the general notion of antiperiodic state, formation of coherent antiperiodic steady states (solitons), where the FH and SH envelopes move with a common velocity without shape changes, characterization of the family of antiperiodic steady states, and the dependence of comb spectra on the pump power and the group velocity difference.

Frequency combs [1, 2] consisting of equidistant optical lines are indispensable for metrology, spectroscopy, and other applications [3–5]. During the last decade, microresonator comb concept becomes increasingly important. Generation of high-quality frequency combs in  $\chi^{(3)}$  microresonators, see [6–13] and references therein, is one of the most spectacular recent achievements in nonlinear optics. These combs correspond to continuous-wave single-frequency pumped coherent spatial structures circulating along the resonator rim with a constant speed. Typically, these structures are dissipative solitons balancing not only dispersion broadening and nonlinearity, but also external pumping and internal losses [10, 13]. They can be substantially different from solitons in conservative systems. The outstanding comb properties are due to high  $Q$ -factors and small volumes of the resonator modes.

Transfer of the comb concept to  $\chi^{(2)}$  resonators represents a big challenge and offers new opportunities. Here, there are two light envelopes – the first and second harmonics (FH and SH) – instead of one and, therefore, two dispersion coefficients. Also there is a substantial group velocity difference leading to the spatial walk-off between FH and SH. Furthermore, phase matching has to be ensured for the second-order nonlinear processes. Realization of  $\chi^{(2)}$  combs promises lowering the pump power, entering new spectral ranges, and new operation regimes. In particular, the presence of two subcombs in the FH and SH spectral ranges, see Fig. 1, is a new positive feature.

First attempts were undertaken to explore soliton regimes relevant to the frequency combs in  $\chi^{(2)}$  resonators [14–16]. They concern with quadratic nonlinear processes running at the spectral point of equal FH and SH group velocities. The found dissipative solitons show a close relation to the conservative solitons reviewed in [17]. Walk-off controlled soliton solutions at nonzero

pump and zero losses were found [18]; their stability is an open issue. Also, numerical results on analysis of comb regimes regardless of solitons are known [19–22]. The overall physical pattern of  $\chi^{(2)}$  combs remains obscure.

In this Letter, we report on walk-off controlled comb solutions for  $\chi^{(2)}$  resonators incorporating pump and losses and applicable to broad spectral ranges of the pump frequency. The found solutions belong to the class of antiperiodic states, including solitons, which are topologically different from conventional periodic states. Also they are totally different from solutions of [18]. The comb generation is stable against small and large perturbations, it can start from noise.

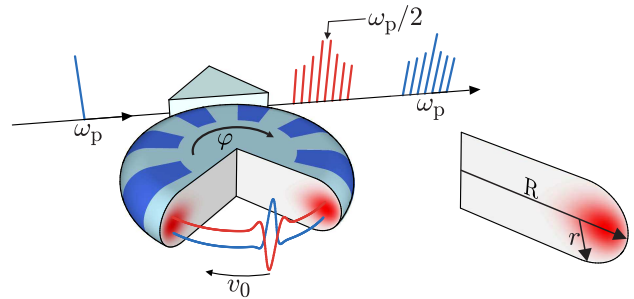


FIG. 1: Schematic of  $\chi^{(2)}$  comb generation. Continuous-wave pump at the frequency  $\omega_p$  generates coupled SH and FH combs in a microresonator owing to cascaded second-order nonlinear processes. These combs correspond to SH and FH solitons moving along the resonator rim with a common velocity  $v_0$ . Red spots show localization of the resonator modes;  $\varphi$  is the azimuth angle. Radial poling and rim shaping via control of the ratio of major ( $R$ ) and minor ( $r$ ) radii allow for quasi-phase matching and mode management, respectively.

High- $Q$  microresonators possess discrete frequency spectra [23–25]. Optical modes of a resonator with major radius  $R$  can be viewed as quasi-plane waves propagating along the resonator rim and characterized by

the azimuth angle  $\varphi$  [23–25], see Fig. 1. The modal functions are  $2\pi$ -periodic. Following all known theoretical comb studies, we restrict ourselves to a single transverse mode type; this implies reducing transverse mode number via rim shaping. Each mode is characterized by the azimuth number  $m$  or by the wavenumber  $k_m = m/R$ . For typical  $\chi^{(2)}$  resonators,  $m \sim 10^4$ , and  $k_m$  form a quasi-continuous set. The modal frequencies are  $\omega_m = 2\pi c/\lambda_m = k_m c/n(\lambda_m)$ , where  $c$  is speed of light,  $\lambda_m$  the vacuum wavelength, and  $n(\lambda)$  the effective refractive index slowly varying with  $\lambda$ . It is close to the bulk index  $n_b(\lambda)$ , but includes corrections relevant to the geometric dispersion and vectorial coupling [26–29].

For quadratic nonlinearity, the phase-matching (PM) conditions  $\omega_{k_2} = \omega_{k_1} + \omega_{k'_1}$ ,  $k_2 = k_1 + k'_1$  with discrete wavenumbers have to be fulfilled. At  $k_1 = k'_1$  they give the SH generation conditions. The latter are fulfilled in exceptional cases [30]. However, equivalent quasi-PM conditions can be ensured via the radial poling, see also Fig. 1 and Supplemental Materials 1 (SM1), practically for any spectral range [31, 32]. This admits the presence of small frequency differences, such that  $|\omega_{2k_1} - 2\omega_{k_1}| \ll c/nR$ . Continuous fine PM tuning means are also available [25, 33, 34].

Let the PM conditions  $\omega_{k_2^0} = 2\omega_{k_1^0}$ ,  $k_2^0 = 2k_1^0$  be fulfilled and the pump frequency  $\omega_p$  be very close to  $\omega_{k_2^0}$  (SH pumping). This means that the azimuth number  $m_2^0$  is even and  $m_1^0 = m_2^0/2$  is an integer, see also Fig. 2a. The true light electric field can be represented as

$$S \exp[i(m_2^0 \varphi - \omega_p t)] + F \exp[i(m_2^0 \varphi - \omega_p t)/2] + c.c., \quad (1)$$

where  $F(\varphi, t)$  and  $S(\varphi, t)$  are complex FH and SH envelopes, both  $2\pi$ -periodic in  $\varphi$ . These envelopes obey a generic set of nonlinear equations [15, 17, 18]:

$$\begin{aligned} \left[ i \left( \frac{\partial}{\partial t} + \frac{v_1}{R} \frac{\partial}{\partial \varphi} + \gamma_1 \right) + \frac{v'_1}{2R^2} \frac{\partial^2}{\partial \varphi^2} - \Delta_1 \right] F &= 2\mu S F^* \quad (2) \\ \left[ i \left( \frac{\partial}{\partial t} + \frac{v_2}{R} \frac{\partial}{\partial \varphi} + \gamma_2 \right) + \frac{v'_2}{2R^2} \frac{\partial^2}{\partial \varphi^2} - \Delta_2 \right] S &= \mu F^2 + ih. \end{aligned}$$

Here  $v_{1,2}$  and  $v'_{1,2}$  are the group velocities and the dispersions (discrete equivalents of  $d\omega/dk$  and  $d^2\omega/dk^2$ ) at  $k_{1,2}^0$ ,  $\gamma_{1,2}$  are the modal decay constants,  $\Delta_{1,2}$  are the frequency detunings accounting for a slightly imperfect PM and a small difference  $\omega_p - \omega_{k_2^0}$ ,  $\mu$  is the coupling constant proportional to the second-order nonlinear coefficient, and  $h$  is the pump strength. These parameters are real and experimentally controlled; the ratios  $v_{1,2}/2\pi R$  ( $\gtrsim 10$  GHz) are known as FH and SH free spectral ranges.

Now let us pump a SH mode with an odd azimuth number  $m_2^0$ , see also Fig. 2b. The PM conditions link this mode to two FH modes possessing even and odd numbers:  $\omega_{m_2^0} = \omega_{m_1^0} + \omega_{m_1^0+1}$ ,  $m_2^0 = 2m_1^0 + 1$ . Is set (2) for  $F$  and  $S$ , as defined by Eqs. (1), valid in this case? The answer is *yes*, but the FH envelope becomes antiperiodic,  $F(\varphi) = -F(\varphi + 2\pi)$ . This follows

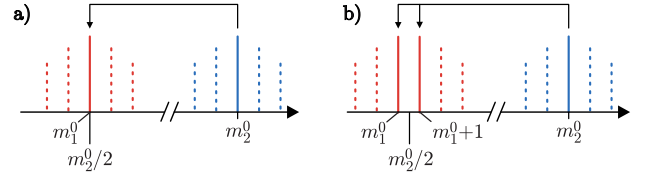


FIG. 2: Excitation of periodic (a) and antiperiodic (b) states at SH-pumping of even and odd modes. The FH carrier frequency  $m_2^0/2$  is integer in a) and semi-integer in b). Side harmonics arise automatically in b) above the threshold.

from  $2\pi$ -periodicity of the true light field and the presence of the antiperiodic factor  $\exp(im_2^0\varphi/2)$  in Eq. (1). The  $2\pi$ -periodic squared modulus  $|F|^2$  still represents the true FH field intensity, while the Fourier expansion of  $F(\varphi)$  consists of semi-integer harmonics  $F_{j_1}$  with  $j_1 = m_1 - m_1^0 - 1/2 = \pm 1/2, \pm 3/2, \dots$ . The SH amplitude  $S(\varphi)$  remains  $2\pi$ -periodic; it includes only integer harmonics  $S_{j_2}$  with  $j_2 = m_2 - m_2^0 = 0, \pm 1, \dots$ . Attempts to employ  $2\pi$ -periodic FH envelopes break the generic structure of Eqs. (2). Further details can be found in SM2 and [18].

The antiperiodic solutions of Eqs. (2) are topologically different from the periodic ones. They form a separate class of nonlinear states, which is specific for SH pumping and favorable for comb generation. The differences between the periodic and antiperiodic states are crucial: – In the periodic case, there are spatially uniform solutions  $\bar{F}(\varphi), \bar{S}(\varphi) = const.$  In the antiperiodic case, such solutions are impossible. Nevertheless,  $\bar{F}$  and  $\bar{S}$  represent here asymptotic almost  $\varphi$ -independent values of  $F(\varphi)$  and  $S(\varphi)$ , see below.

– Harmonics  $F_{1/2}$  and  $F_{-1/2}$  not only influence  $S_0$ , but force harmonics  $S_{\pm 1}$  enriching the SH spectrum. The latter cause new nonlinear processes, so that a broad FH spectrum appears above a single oscillation threshold.

Nonlinear set (2), including many variable parameters, is generally very complicated. In particular, it is more complicated compared to the Lugiato-Lefever equation [35, 36] relevant to  $\chi^{(3)}$  comb modeling [10, 13]. We restrict ourselves to the case of zero detunings  $\Delta_{1,2} = 0$ . This means that the PM conditions are fulfilled exactly. Also, we set for simplicity  $\gamma_{1,2} = \gamma$ . Four dimensionless parameters control then the nonlinear behavior. These are the normalized pump strength  $\eta = 2\mu h/\gamma^2$ , the walk-off parameter  $\alpha = v_{12}/\gamma R$  with  $v_{12} = v_1 - v_2$ , and two dispersion parameters  $\beta_{1,2} = v'_{1,2}/2\gamma R^2$ .

Importance of different parameters and the physical pattern can be clarified taking into account representative dependences  $v_{1,2}(\lambda)$  and  $v'_{1,2}(\lambda)$ , see Fig. 3. For mm-sized resonators, the effects of geometric dispersion are weak. The group velocity difference  $v_{12} = v_1 - v_2$  ranges from huge values ( $\sim 10^8$  cm/s) to zero at  $\lambda_2^0 \simeq 1.36 \mu\text{m}$ . Setting  $R = 1.5$  mm,  $\gamma = 10^7$  s $^{-1}$  ( $Q \approx 10^8$ ), we get for the pump wavelength  $\lambda_2 \simeq 1 \mu\text{m}$ :  $\alpha \approx 2 \times 10^2$ ,

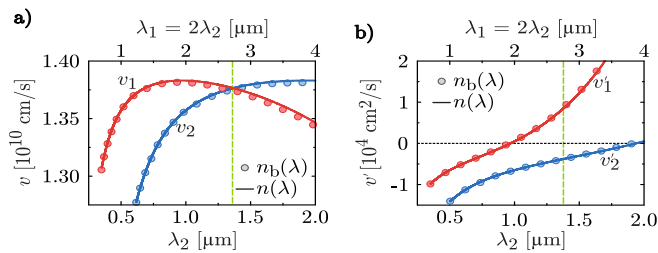


FIG. 3: Wavelength dependences of the group velocities  $v_{1,2}$  (a) and the dispersions  $v'_{1,2}$  (b) for lithium niobate based resonator with  $R = 1.5$  mm and  $R/r = 3$ . The solid and dotted lines refer to the bulk refractive index  $n_b$  and the effective index  $n$  incorporating the effects of geometric dispersion. The vertical lines  $\lambda = \lambda_2^0 = \lambda_1^0/2 \simeq 1.36 \mu\text{m}$  correspond to  $v_1 = v_2$ .

$\beta_1 \approx 3 \times 10^{-3}$ , and  $\beta_2 \approx -3 \times 10^{-2}$ . This means that the walk-off effects dominate over the dispersion ones. When moving to the point of equal group velocities  $\lambda_2^0$ , the coefficient  $\alpha$  tends to zero, while  $\beta_1$  and  $\beta_2$  remain opposite in sign with  $|\beta_{1,2}| \approx 10^{-2}$ . Thus, the walk-off effects can be controlled by the choice of the pump wavelength  $\lambda_2$ ; they are small in the close vicinity of  $\lambda_2^0$ . The threshold value of  $\eta$  for generation of the antiperiodic states is  $\eta_{\text{th}} = (1 + \beta_1^2/16)^{1/2} \simeq 1$ , see also SM2. For the periodic states, it is  $\eta_{\text{th}} = 1$ . Thus,  $\eta$  is expressible by the ratio of the pump power  $\mathcal{P}$  to its threshold value:  $\eta^2 = \mathcal{P}/\mathcal{P}_{\text{th}}$ .

Above the threshold, we are eager for steady states  $F(\varphi - v_0 t/R)$ ,  $S(\varphi - v_0 t/R)$  moving with a common velocity  $v_0$  without shape changes. Only such states provide FH and SH frequency combs; the Fourier components  $F_{j_1}$  and  $S_{j_2}$  represent here the FH and SH frequency spectra with the common frequency spacings  $\delta\omega = v_0/R$ . Periodic steady states with such frequency spacing are not expected for  $\Delta_{1,2} = 0$ : The spatially uniform solution  $\bar{F}, \bar{S}$  with  $|\bar{F}|^2 \propto \eta - \eta_{\text{th}}$  is known to be stable here against spatially uniform and quasi-uniform perturbations. The *antiperiodic* steady states provide potentially the best possibility for comb generation. The presence of such states and their stability against temporal perturbations are not granted. Also, velocity  $v_0$  is unknown, it must be determined simultaneously with the shape of the steady states. Since the parametrically generated satellites  $F_{\pm 1/2}$  propagate at the threshold with velocity  $v_1$  and force an SH pattern propagating with the same velocity, we expect that  $v_0 \simeq v_1$  near the threshold. The velocity difference  $v_{01} = v_0 - v_1$  is an important parameter; the ratio  $v_{01}/2\pi R$  characterizes fine nonlinear tuning of the comb frequency spacing.

We simulated numerically the Fourier transform of Eqs. (2) at  $\Delta_{1,2} = 0$  in the coordinate frame moving with velocity  $v_1$  using the fourth-order Runge-Kutta method. The total number of harmonics taken into account ranged from 64 to 512. The harmonics  $F_{j_1}(t)$  and  $S_{j_2}(t)$  were found within a large range of  $j_{1,2}$  and within a sufficiently broad range of  $\eta$ ,  $\alpha$ :  $1 \leq \eta \leq 100$ ,  $10^{-2} \leq \alpha \leq 10^2$ . Ac-

curacy of the calculations was controlled by changing the time step and the total number of harmonics. With the harmonics calculated, one can ensure establishment of the antiperiodic steady states and determine the velocity difference  $v_{01}$ , the comb spectra  $|F_{j_1}|^2$  and  $|S_{j_2}|^2$ , and the spatial profiles  $F(\varphi, t)$ ,  $S(\varphi, t)$ .

The following quasi-adiabatic calculation procedure was used to cover the whole  $\eta, \alpha$  range: Parameter  $\eta$  increased and decreased stepwise at certain  $\alpha$ , and the previous values of  $F_{j_1}$  and  $S_{j_2}$  were used as new initial conditions. Achievement of steady states was controlled in each step. It was found that the result of temporal evolution does not depend on the initial conditions (including random noise). It is arrival at a unique coherent FH-SH pattern moving with a common velocity  $v_0(\alpha, \eta)$ . The sufficient restriction on the pump rise time  $t_p$  is  $t_p \gtrsim 1 \mu\text{s}$ ; it is very soft. The found features mean that the comb generation is self-starting. More details can be found in SM3. Note that adiabatic changes of  $\eta$  (of the pump power) are practical for experiment, whereas big adiabatic changes of  $\alpha$  would be impractical.

Turning to the results, we start with dependences of the comb spectra on  $\alpha$  and  $\eta$ . For the FH and SH amplitudes, it is convenient to use the normalized quantities  $f = (\mu/\gamma)(2i)^{1/2}F$  and  $s = (2\mu/\gamma)S$ . With this normalization, the spatially uniform steady states are given by  $\bar{f} = \pm(\eta - 1)^{1/2}$  and  $\bar{s} = 1$ . This sets a useful reference scale. While all harmonics are nonzero in steady state, we restrict ourselves to the range  $|f_{j_1}|^2, |s_{j_2}|^2 \geq 10^{-4}$  when presenting the comb spectra. The corresponding numbers of significant FH and SH comb lines we denote  $N_1$  and  $N_2$ .

Figure 4 shows the normalized comb spectra for two combinations of  $\eta$  and  $\alpha$  and the dispersion parameters  $\beta_1 = 0.02$ ,  $\beta_2 = -0.01$ . For  $\alpha = 50$  and  $\eta = 100$ , representing large  $\alpha$  and  $\eta$ , we have  $N_1 = 33$ ,  $N_2 = 19$ , see Figs. 4a,b, a very small positive velocity ratio  $v_{01}/v_{12} \approx 10^{-3}$ , and  $v_{01}/2\pi R \approx 0.1$  MHz. In the SH spectrum there is one dominating line,  $|s_0|^2 \simeq 1$ . For  $\alpha = 1/12$  and  $\eta = 25$ , representing small walk-off parameters and modest pump strengths, we have well developed FH and SH spectra with  $N_1 = 79$  and  $N_2 = 88$ , see Figs. 4c,d, corresponding to  $v_{01}/v_{12} \approx 3.4$  and  $v_{01}/2\pi R \approx 0.45$  MHz. Domination of  $|s_0|^2$  over the SH wings is much less pronounced. The left-right asymmetry of the spectra of Fig. 4c,d and their ripple structure are remarkable; these features are due to an interplay between the walk-off and dispersion effects.

Next, we consider the tuning parameter  $v_{01}/2\pi R$  and the total number of comb lines  $N_1 + N_2$  as functions of  $\alpha^{-1}, \eta$  within the range  $0.1 \leq \alpha^{-1} \leq 50$ ,  $1 \leq \eta \leq 30$ , see Fig. 5. A remarkable feature is here the presence of the vertical line of discontinuity  $\alpha = \alpha_c \simeq 1/13$ ,  $\eta > \eta_c \simeq 4.5$ .

Both mapped quantities grow with increasing  $\eta$ , but this growth is substantially weaker for  $\alpha < \alpha_c$ . Taken as

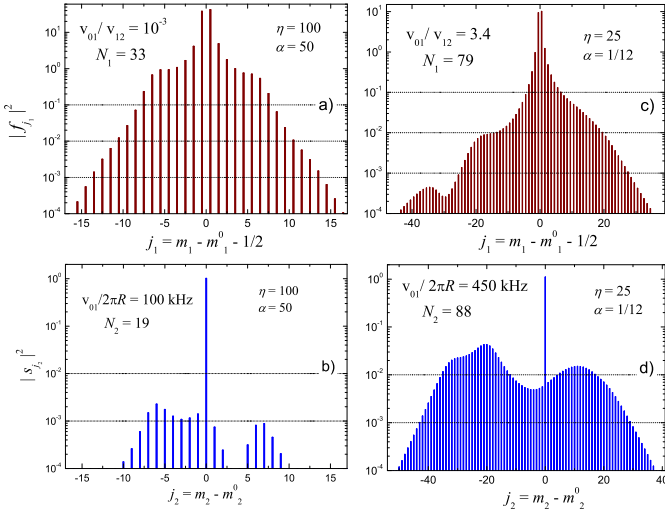


FIG. 4: Steady-state comb spectra  $|f_{j_1}|^2$  and  $|s_{j_2}|^2$  for two combinations of  $\eta$  and  $\alpha$  and the dispersion parameters  $\beta_1 = 0.02$  and  $\beta_2 = -0.01$ . a),b):  $\eta = 100$  and  $\alpha = 50$ ; c),d):  $\eta = 25$  and  $\alpha = 1/12$ . Only the comb lines above  $10^{-4}$  are shown. The total number of Fourier harmonics taken into account is 128 for a),b) and 512 for c),d). The frequency spacing between the lines is  $\delta\omega = v_0/R$ .

functions of  $\lg(1/\alpha)$ , they grow first approximately linearly and then drop and stop growing. The drops in a) and b) are relatively large and small. Furthermore,  $v_{01}$  tends to zero for  $\alpha \rightarrow 0$ . In essence, the discontinuity marks a sharp transition from the walk-off to dispersion controlled comb regimes for  $\eta > \eta_c$ . For  $\eta < \eta_c$ , this transition occurs continuously with increasing  $\lg(1/\alpha)$ . When moving up along the left side of the discontinuity, the tuning parameter approaches the MHz range for  $\eta \approx 30$ , and the values of  $v_{01}/v_{12}$  and  $N_1 + N_2 \simeq 2N_1$  approach 3.4 and 180, respectively. Further increase of  $\eta$  presents no numerical difficulties, but can lead to excessively large pump powers. Minor irregularities of the map b) are caused by discreteness of  $N_{1,2}$  and by the ripple structure of the comb spectra: small variations of  $\eta$  and  $\alpha$  cause sometimes stepwise changes of these integers.

Consider the spatial structure of our antiperiodic steady states. Figure 6 shows the FH and SH intensities and phases versus the azimuth angle  $\varphi$  for points **1** and **2** on the  $\alpha^{-1}, \eta$  plane lying slightly to the left and right of the discontinuity in Fig. 5. It is evident from a) and c) that the intensity changes are strong and well localized, so that we are dealing with FH and SH solitons propagating with velocity  $v_0$ . Each intensity distribution has a background; in accordance with the previous considerations, the FH and SH intensity backgrounds are  $\bar{f}^2 = \eta - 1$  and  $\bar{s}^2 = 1$ . The intensity profiles **1** are much more oscillatory as compared to profiles **2**. The phase  $\arg[f(\varphi)]$  exhibits sharp  $\pi$ -steps in both cases ensuring the antiperiodic behavior. The behavior of  $\arg[s(\varphi)]$  is, however, not uniform: the phase profiles **1** and **2** in

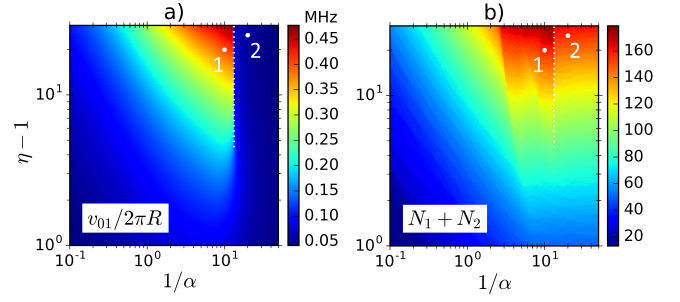


FIG. 5: Maps of the tuning parameter  $v_{01}/2\pi R$  (a) and of the total number of significant comb lines  $N_1 + N_2$  (b) on the  $\alpha^{-1}, \eta$  plane for  $\beta_1 = 0.02$  and  $\beta_2 = -0.01$ . The vertical line of discontinuity starts at  $1/\alpha_c \simeq 13$ ,  $\eta_c \simeq 4.5$ . Each map incorporates the data of  $151 \times 151 = 22801$  calculation variants with 512 harmonics taken into account. White dots **1** and **2** correspond to the points of the plane (10, 20) and (20, 25) lying to the left and right of the discontinuity and also to profiles **1** and **2** in Fig. 6.

Fig. 6d show  $2\pi$ -drop and a zero overall change.

What happens with the solitons when changing  $\eta, \alpha$ ? Decrease of  $\alpha$  as compared to  $\alpha_c$  gives no effect, the profiles **2** in Fig. 6 correspond practically to the limit  $\alpha \rightarrow 0$ . Increasing  $\alpha$  causes a weak bifurcation of soliton **1**: the  $2\pi$ -drop of  $\arg(s)$  changes to 0. This bifurcation is not accompanied by discontinuities of  $v_{01}$  and  $N_{1,2}$ .

Above we focused on the spectral range  $\lambda_2 < \lambda_2^0 \simeq 1.36 \mu\text{m}$ , where  $v_{12}(\lambda_2) > 0$ , see Fig. 3. Generalization to the range  $\lambda_2 > \lambda_2^0$ , where  $v_{12} < 0$ , presents no difficulties. It results in changing sign of  $v_{01}$ . Modest variations of the dispersions  $\beta_{1,2}$  and of the ratio  $\gamma_1/\gamma_2$  influence

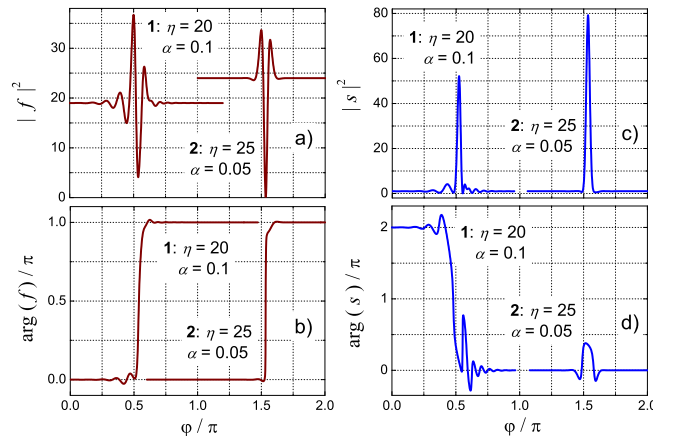


FIG. 6: Antiperiodic solitons for points **1** and **2** lying to the left and right of the discontinuity in Fig. 5. Sub-figures a) to d) show  $|f(\varphi)|^2$ ,  $\arg[f(\varphi)]$ ,  $|s(\varphi)|^2$ , and  $\arg[s(\varphi)]$ . The background values of  $|f|^2$  and  $|s|^2$  are  $\eta - 1$ , and 1, respectively. The  $\pi$ -steps of  $\arg[f(\varphi)]$  in b) occur at the points of minimum of  $|f(\varphi)|^2$  in a). Changes of  $\arg[s(\varphi)]$  occur near the maxima of  $|s(\varphi)|^2$ , they are qualitatively different for **1** and **2**. 512 FH and SH harmonics are taken into account.

quantitative details, but not the physical pattern.

How precise and informative is our assertion about achievement of the steady states? To clarify it, we introduce the discrepancy parameter

$$\varepsilon(t, \tau) = \frac{\sum_j |A_j(t) - A_j(t - \tau)|^2}{\sum_j (|A_j(t)|^2 + |A_j(t - \tau)|^2)}, \quad (3)$$

where  $A_j$  is one of the harmonics  $F_{j_1}$  and  $S_{j_2}$  in the frame moving with an arbitrary velocity  $v$ ,  $t$  is the calculation time, and  $\tau$  is a variable time shift. As soon as harmonics  $A_j(t)$  are known in the frame moving with velocity  $v_1$ , they can be recalculated in the frame moving with velocity  $v$  through multiplication by  $\exp[-ij_{1,2}(v - v_1)t/R]$ . Obviously,  $\varepsilon(t, \tau)$  turns to zero only when we deal with the steady state and, simultaneously,  $v = v_0$ . The discrepancy parameter calculated for modestly large evolution times,  $\gamma t \gtrsim 10^3$ , and minimized over  $v$  shows extremely small values ( $\varepsilon = 10^{-14} - 10^{-15}$ ) caused by the numerical noise, see [SM3](#) for details. For smaller  $t$ , i.e., during the transient stage, it is larger by many orders of magnitude. Thus, we have a tool to control proximity of the steady states and to determine precisely velocity  $v_0$ .

For  $\eta \gg 1$  and an abrupt (non-adiabatic) turning of the pump on, the above scenario of nonlinear evolution to unique steady states can be violated. In this case, generation of single-soliton steady states from noise occurs probabilistically, and complicated multi-soliton structures become most probable.

Turning to discussion, we consider first the main distinctive features of this study:

- The results found for  $\chi^{(2)}$  resonators concern with new antiperiodic nonlinear comb states that are topologically different from conventional periodic states. To excite the antiperiodic states, it is sufficient to pump SH modes with odd azimuth numbers. Neither  $\chi^{(3)}$  nor FH pumped  $\chi^{(2)}$  resonators possess such states. The antiperiodic states are the most favorable for  $\chi^{(2)}$  comb generation: Formation of broad spectra of Fourier harmonics occurs automatically above a single optical oscillation threshold, while spatially-uniform background states are forbidden.

- The necessary condition for the generation of equidistant  $\chi^{(2)}$  frequency combs, formation of FH and SH envelopes propagating with a common constant velocity without shape changes, is fulfilled in broad ranges of experimental parameters, such as pump wavelength and power. Moreover, the comb states are self-starting – the nonlinear evolution leads above the threshold to a unique comb state under weak limitations on the pump rise time.

- In contrast to the previous  $\chi^{(2)}$  comb studies [14–16], we are not attached to the spectral point of equal FH and SH group velocities  $\lambda_2^0$ . The spatial walk-off of the FH and SH envelopes, caused by generic group velocity difference, controls the spectral features of the comb

solutions together with the pump power.

- Broad comb spectra correspond to a vast family of spatially narrow antiperiodic dissipative solitons. These solitons not only balance the dispersion broadening and nonlinear narrowing, gain and losses, but also ensure a common velocity of FH and SH envelopes. To the best of our knowledge, this multiparametric soliton family has no analogues in the literature.

While the single-mode and perfect radial poling assumptions are realistic and common for the theoretical comb studies, they are not always fulfilled in experiment. Special efforts are necessary thus for the experimental realization of  $\chi^{(2)}$  combs. As concern our assumption of zero FH and SH frequency detunings, it is made for simplicity. On the one hand, it is realizable in experiment. On the other hand, admission of nonzero detunings is expected to strongly complicate the comb regimes. Possibly, it will result in new important predictions for experiment.

In conclusion, the presented theoretical results form a broad and solid frame for practical realization of frequency combs in  $\chi^{(2)}$  microresonators. They have a big potential for further extension by incorporating the effects of FH and SH frequency detunings.

**Acknowledgements:** This work was financially supported by RFBR, grant number 20-02-00511, and by the Fraunhofer and Max Planck Cooperation Program COSPA

- 
- [1] T. Udem, R. Holzwarth, and T. W. Hansch, *Nature (London)* **416**, 233 (2002).
  - [2] *Femtosecond Optical Frequency Comb Technology*, edited by J. Ye and S. T. Cundiff (Springer, New York, 2005).
  - [3] L. Ma, Z. Bi, A. Bartels, L. Robertsson, M. Zucco, R. Windeler, G. Wilpers, C. Oates, L. Hollberg, and S. A. Diddams, *Science* **303**, 1843 (2004).
  - [4] M. J. Thorpe, K. D. Moll, J. J. Jones, B. Safdi, and J. Ye, *Science* **311**, 1595 (2006).
  - [5] S. A. Diddams, L. Hollberg, and V. Mbele, *Nature (London)* **445**, 627 (2007).
  - [6] P. Del’Haye, A. Schliesser, O. Arcizet, T. Wilken, R. Holzwarth, and T. J. Kippenberg, *Nature* **450**, 1214 (2007).
  - [7] T. Herr, E. Gavartin, M. L. Gorodetsky, R. Holzwarth, and T. J. Kippenberg, *Phys. Rev. Lett.* **107**, 063901 (2011).
  - [8] T. J. Kippenberg, R. Holzwarth, and S. A. Diddams, *Science* **332**, 555 (2011).
  - [9] T. Herr, K. Hartinger, J. Riemensberger, C. Y. Wang, E. Gavartin, R. Holzwarth, M. L. Gorodetsky, and T. J. Kippenberg, *Nat. Photonics* **6**, 480 (2012).
  - [10] T. Herr, V. Brasch, J. D. Jost, C. Y. Wang, N. M. Kondratiev, M. L. Gorodetsky, and T. J. Kippenberg, *Nat. Photonics* **8**, 145 (2014).
  - [11] X. Yi, Q.-F. Yang, M.-J. Suh, and K. Vahala, *Optica* **2**,

- 1078 (2015).
- [12] M. G. Suh and K. Vahala, *Optica* **5**, 65 (2018).
- [13] T. J. Kippenberg, A. L. Gaeta, M. Lipson, and M. L. Gorodetsky, *Science* **361**, 567 (2018).
- [14] T. Hansson, P. Parra-Rivas, M. Bernard, F. Leo, L. Gelsen, and S. Wabnitz, *Opt. Lett.* **43**, 6033 (2018).
- [15] A. Villosio and D. Skryabin, *Opt. Express* **27**, 7098 (2019).
- [16] A. Villosio N. Kondratiev, I. Breunig, D. N. Puzyrev, and D. V. Skryabin, *Opt. Lett.* **44**, 4443 (2019).
- [17] A. V. Buryak, P. Di Trapani, D. V. Skryabin, and S. Trillod, *Phys. Rep.* **370**, 63 (2002).
- [18] E. Podivilov, S. Smirnov, I. Breunig, and B. Sturman, Submitted (arXiv 1910.03397).
- [19] V. Ulvila, C. R. Phillips, L. Halonen, and M. Vainio, *Opt. Express* **22**, 10535 (2014).
- [20] F. Leo, T. Hansson, I. Ricciardi, M. De Rosa, S. Coen, S. Wabnitz, and M. Erkintalo, *Phys. Rev. Lett.* **116**, 033901 (2016).
- [21] S. Mosca, I. Ricciardi, M. Parisi, P. Maddaloni, L. Santamaria, P. De Natale, and M. De Rosa, *Nanophotonics* **5**, 316 (2016).
- [22] S. Mosca, M. Parisi, I. Ricciardi, F. Leo, T. Hansson, M. Erkintalo, P. Maddaloni, P. De Natale, S. Wabnitz, and M. De Rosa, *Phys. Rev. Lett.* **121**, 093903 (2018).
- [23] K. J. Vahala, *Nature* **424**, 839 (2003).
- [24] V. S. Ilchenko and A. B. Matsko, *Quantum Electron.* **12**, 15 (2006).
- [25] D. Strelkalov, Ch. Marquardt, A. B. Matsko, H. G. L. Schwefel, and G. Leuchs, *J. Opt.* **18**, 123002 (2016).
- [26] M. Gorodetsky and A. Fomin, *J. Sel. Top. Quantum Electron.* **12**, 33-39 (2006).
- [27] M. L. Gorodetsky and Y. A. Demchenko, *Proc. SPIE* **8236**, 823623 (2012).
- [28] I. Breunig, B. Sturman, F. Sedlmeir, H. G. L. Schwefel, and K. Buse, *Opt. Express* **21**, 30683 (2013).
- [29] B. Sturman, E. Podivilov, C. S. Werner, and I. Breunig, *Phys. Rev. A* **99**, 013810 (2019).
- [30] J. U. Fürst, D. V. Strelkalov, D. Elser, M. Lassen, U. L. Andersen, C. Marquardt, and G. Leuchs, *Phys. Rev. Lett.* **104**, 153901 (2010).
- [31] T. Beckmann, H. Linnenbank, H. Steigerwald, B. Sturman, D. Haertle, K. Buse, and I. Breunig, *Phys. Rev. Lett.* **106**, 143903 (2011).
- [32] M. Mohageg, D. V. Strelkalov, A. A. Savchenkov, A. B. Matsko, V. S. Ilchenko, and L. Maleki, *Opt. Express* **13**, 3408 (2005).
- [33] Ch. Werner, W. Yoshiki, S. Herr, I. Breunig, and K. Buse, *Optica* **4**, 1205 (2017).
- [34] S. Meisenheimer, J. Frst, K. Buse, and I. Breunig, *Optica* **4**, 189 (2017).
- [35] L. A. Lugiato and R. Lefever, *Phys. Rev. Lett.* **58**, 2209 (1987).
- [36] I. V. Barashenkov and Yu. S. Smirnov, *Phys. Rev.* **54**, 5707 (1996).

# Supplemental Materials to Walk-off Controlled Self-Starting Frequency Combs in $\chi^{(2)}$ Optical Microresonators

S. Smirnov<sup>1</sup>, B. Sturman<sup>2</sup>, E. Podivilov<sup>1,2</sup>, and I. Breunig<sup>3,4</sup>

<sup>1</sup>*Novosibirsk State University, 630090, Novosibirsk, Russia*

<sup>2</sup>*Institute of Automation and Electrometry, Russian Academy of Sciences, 630090 Novosibirsk, Russia*

<sup>3</sup>*University of Freiburg, Department of Microsystems Engineering - IMTEK,  
Georges-Köhler-Allee 102, 79110 Freiburg, Germany*

<sup>4</sup>*Fraunhofer Institute for Physical Measurement Techniques, 79110 Freiburg, Germany*

(Dated: March 4, 2022)

## I. THE EFFECT OF RADIAL POLING

The nonlinear response of ferroelectric  $\chi^{(2)}$  materials, like LiNbO<sub>3</sub> or LiTaO<sub>3</sub>, is determined by the independent real  $d_{333}$  and  $d_{311}$  components of the third-rank quadratic susceptibility tensor  $\hat{d}$  [1]. These components change sign under inversion of the direction of the spontaneous polarization. In the case of perfect radial poling, shown schematically in Fig. 1 of the main text, any of these components (let it be  $d$  with the bulk value  $d_{\text{bulk}}$ ) alternates periodically in a stepwise manner with the azimuth angle  $\varphi$ , as illustrated in Fig. 1a. At the same time, the linear susceptibility tensor and the linear optical properties stay unchanged. If  $N$  is the number of alternation periods, the function  $d(\varphi)$  is  $2\pi/N$ -periodic. It can be expanded in the Fourier series

$$d = \sum_j d_j \exp(ij\varphi), \quad (1)$$

with  $j = 0, \pm N, \pm 2N, \dots$ . In the case of  $\pm$ -symmetric radial domain structure, which is the most suitable for quasi-phase matching, only the Fourier harmonics with odd ratios  $j/N = \pm 1, \pm 3, \dots$  are nonzero [2, 3]. For these harmonics we have  $|d_j| = 2d_{\text{bulk}}N/\pi|j|$ . The reduction factor  $|d_j|/d_{\text{bulk}}$  decreases with increasing  $|j|/N$ , but remains comparable with 1 for  $|j| = N$ , see also Fig. 1b.

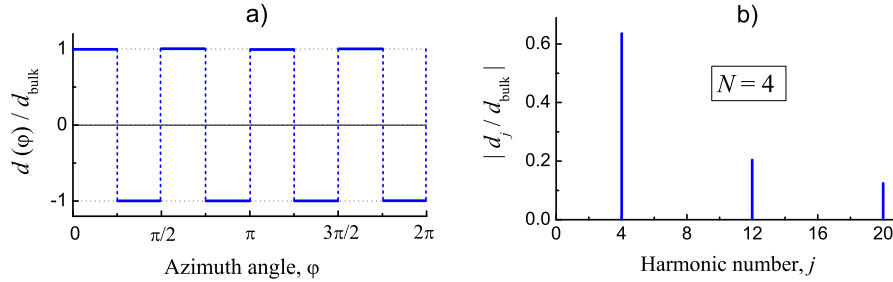


FIG. 1: a) Schematic of the azimuth dependence of the susceptibility coefficient  $d(\varphi)$  for a perfect symmetric radial domain pattern with  $N = 4$ . b) First three harmonics of the corresponding Fourier spectrum with  $j = N, 3N$ , and  $5N$ .

Employment of the first Fourier harmonics of  $d(\varphi)$  for quasi-phase matching corresponds to the SH phase-matching conditions  $2\omega_{m_1} = \omega_{2m_1 \pm N}$ . The sign "plus" is relevant to the most typical case of decreasing wavelength dependence of the refraction index  $n(\lambda)$  [4]. We see that the SH azimuth number  $m_2 = 2m_1 \pm N$  is even for even alternation number  $N$  and odd for odd number  $N$ . In this case, SH pumping leads to the excitation of periodic states. In the case of odd combination  $m_2 \mp N$ , the SH quasi-phase matching condition cannot be fulfilled. However, we can fulfil the quasi-phase matching condition  $\omega_{m_1} + \omega_{m_1+1} = \omega_{2m_1 \pm N}$  leading to the excitation of the antiperiodic states. The values of  $N$  typical for the radial poling are of the order of  $10^2$  [2, 5].

Thus, employment of perfect radial poling leads merely to the replacement of the SH azimuth number  $m_2$  by  $m_2 \mp N$  and to the replacement of the bulk nonlinear coefficient  $d_{\text{bulk}}$  by a slightly reduced coefficient  $d_{\text{eff}} = 2d_{\text{bulk}}/\pi$ . Generally speaking, one can employ the higher Fourier harmonics for quasi-phase matching. At the same number  $N$ , they correspond to substantially different wavelength ranges and also smaller nonlinear coupling coefficients. It is worthy of mentioning that the quasi-phase matching can be combined with continuous fine frequency tuning, such as the temperature tuning or geometric tuning. This enables one to accomplish the quasi-phase matching practically in any desirable spectral range.

Any disturbance of the  $2\pi/N$  periodicity of the radial domain structure leads to decrease of the primary Fourier harmonics  $d_N, d_{3N}, \dots$  and also to additional Fourier harmonics  $d_j$  with  $j \neq N, 3N, \dots$  [2] Strong enough distortions can suppress the primary nonlinear phenomena and cause unwanted parasitic nonlinear processes. The well-spread linear poling in commercially available samples of LiNbO<sub>3</sub> and LiTaO<sub>3</sub> crystals [6, 7], is not appropriate for the comb generation. Among the most dangerous perturbation of the  $2\pi/N$  periodicity is off-centering of the radial domain patterns. It can lead to noticeable side Fourier harmonics neighboring to  $d_N$ . The presence of domain walls in radially poled microresonators can cause additional losses. Nevertheless, the  $Q$  factors in mm-sized resonators reach values  $\sim 10^8$  [2, 8]. Substantially smaller radially poled on-chip resonators possess so far quality factors  $Q \lesssim 10^6$  [9, 10]. Manufacturing of  $\chi^{(2)}$  microresonators with high-quality radial poling and minimized losses can be regarded as a significant step in realization of the  $\chi^{(2)}$  frequency combs.

## II. GOVERNING EQUATIONS FOR THE ANTIPERIODIC STATES

As the starting point for our derivation procedure we use the following generic nonlinear equations for complex modal amplitudes  $F_{m_1}$  and  $S_{m_2}$  relevant to FH and SH frequency ranges, respectively, and pumping into a SH mode with azimuth number  $m_2^0$ :

$$\begin{aligned} i\frac{dF_{m_1}}{dt} - (\omega_{m_1} - i\gamma_{m_1})F_{m_1} &= 2\mu \sum_{m_2, m_1'} S_{m_2} F_{m_1'}^* \delta_{m_2 - m_1 - m_1' - N} \\ i\frac{dS_{m_2}}{dt} - (\omega_{m_2} - i\gamma_{m_2})S_{m_2} &= \mu \sum_{m_1, m_1'} F_{m_1} F_{m_1'} \delta_{m_2 - m_1 - m_1' - N} + ih\delta_{m_2 - m_2^0} e^{-i\omega_p t}. \end{aligned} \quad (2)$$

Here  $\gamma_{m_{1,2}}$  are the modal decay parameters, such that the quality factors  $Q_{m_{1,2}} = \omega_{m_{1,2}}/2\gamma_{m_{1,2}} \gg 1$ ,  $\mu$  is the coupling coefficient incorporating the relevant susceptibility coefficient and modal overlaps [11, 12],  $\omega_p$  is the pump frequency,  $h$  is a variable parameter characterizing pump strength, and the asterisk indicates complex conjugation. The Kronecker symbols express the momentum conservation law in the presence of radial poling. The amplitudes are normalized such that  $\omega_{m_1}|F_{m_1}|^2$  and  $\omega_{m_2}|S_{m_2}|^2$  are the modal energies. Without loss of generality,  $\mu$  and  $h$  can be treated as real positive quantities. The FH and SH modes can be polarizationally the same or different. The case  $N = 0$  corresponds to phase matching of differently polarized modes without radial poling (the natural phase matching [13]). Transfer to the case of FH pumping is evident. The presence of a factor of 2 in Eqs. (2) reflects the Hamiltonian nature of classical  $\chi^{(2)}$  interactions in the absence of modal losses [14]. In essence, set (2) accounts in a general manner for the effects of modal dispersion, decay, dissipativeless  $\chi^{(2)}$  coupling, and frequency selective pumping.

Now we assume that  $m_2^0 - N = 2m_1^0 + 1$  is an odd number. Also we assume that the pump frequency  $\omega_p$  is very close to the SH frequency  $\omega_{m_2^0}$  and  $\omega_{m_2^0}$  is very close to  $\omega_{m_1^0} + \omega_{m_1^0+1}$ . More specifically, we suppose that the pump detuning  $\Delta_p = \omega_{m_2^0} - \omega_p$  and the detuning  $\Delta_q = \omega_{m_1^0} + \omega_{m_1^0+1} - \omega_{m_2^0}$  relevant to a slightly imperfect quasi-phase matching are much smaller in the absolute values as compared to the intermodal distances  $v_{1,2}/R$ . At the same time, these detunings can be comparable with or even larger than the FH and SH line widths  $2\gamma_{m_{1,2}}$ . The detunings  $\Delta_p$  and  $\Delta_q$  can be controlled separately in experiment.

Further simplifications imply relative narrowness of the FH and SH spectra. Let the modal numbers  $m_1$  and  $m_2$  in Eqs. (2) be close to  $m_1^0$  and  $m_2^0$ , respectively, such that the deviations  $\delta m_1 = m_1 - m_1^0$  and  $\delta m_2 = m_2 - m_2^0$  are substantially smaller than  $m_1^0$  and  $m_2^0$ . Then we can employ the Taylor expansions for the modal frequencies

$$\omega_{m_1} = \omega_{m_1^0} + \frac{v_1}{R} \delta m_1 + \frac{v_1'}{2R^2} \delta m_1^2, \quad \omega_{m_2} = \omega_{m_2^0} + \frac{v_2}{R} \delta m_2 + \frac{v_2'}{2R^2} \delta m_2^2, \quad (3)$$

where  $v_{1,2}$  and  $v_{1,2}'$  are the group velocities and the group velocity dispersions for modes  $m_{1,2}^0$ , as defined and quantified in the main text. Analogous discrete expansions are wide-spread in the comb literature, see, e.g., [15–18]. Similar expansions can, generally speaking, be employed for the modal decay parameters  $\gamma_{m_{1,2}}$ . Since the  $m$ -dependences of these parameters are typically less important than the effects of frequency dispersion, we set for simplicity  $\gamma_{m_{1,2}} = \gamma_{1,2} = \text{const}$ .

Using the above assumptions, it is not difficult to obtain evolutionary partial differential equations for true FH and SH envelopes  $\mathcal{F}(\varphi, t)$  and  $\mathcal{S}(\varphi, t)$ , that are given by the Fourier expansions

$$\mathcal{F} = \sum_{\delta m_1} F_{m_1} e^{i\delta m_1 \varphi + i\omega_p t/2} = \sum_{\delta m_1} \tilde{F}_{\delta m_1} e^{i\delta m_1 \varphi}, \quad \mathcal{S} = \sum_{\delta m_2} S_{m_2} e^{i\delta m_2 \varphi + i\omega_p t} = \sum_{\delta m_2} \tilde{S}_{\delta m_2} e^{i\delta m_2 \varphi} \quad (4)$$



and  $2\pi$ -periodic in  $\varphi$ . The slow modal amplitudes  $\tilde{F}_{\delta m_1}$  and  $\tilde{S}_{\delta m_2}$  obey Eqs. (2) if we replace in these equations  $\omega_{m_1} \rightarrow \omega_{m_1} - \omega_p/2$ ,  $\omega_{m_2} \rightarrow \omega_{m_2} - \omega_p$ ,  $\delta_{m_2 - m_1 - m'_1 - N} \rightarrow \delta_{\delta m_2 - \delta m_1 - \delta m'_1 + 1}$  and omit the factor  $\exp(-i\omega_p t)$ . Multiplying the equations for  $\tilde{F}_{\delta m_1}$  and  $\tilde{S}_{\delta m_2}$  by  $\exp(i\delta m_1 \varphi)$  and  $\exp(i\delta m_2 \varphi)$ , respectively, taking the sums in  $\delta m_1$  and  $\delta m_2$ , and employing Eqs. (3), we obtain:

$$\begin{aligned} \left( i\partial_t + i\frac{v_1}{R} \partial_\varphi + \frac{v'_1}{2R^2} \partial_\varphi^2 + \frac{\omega_p}{2} - \omega_{m_1^0} + i\gamma_1 \right) \mathcal{F} &= 2\mu \mathcal{S} \mathcal{F}^* \exp(i\varphi) \\ \left( i\partial_t + i\frac{v_2}{R} \partial_\varphi + \frac{v'_1}{2R^2} \partial_\varphi^2 + \omega_p - \omega_{m_2^0} + i\gamma_2 \right) \mathcal{S} &= \mu \mathcal{F}^2 \exp(-i\varphi) + ih. \end{aligned} \quad (5)$$

Explicit dependences of the right-hand sides on the azimuth angle  $\varphi$  make Eqs. (5) not autonomous and, thus, inconvenient. This feature is a direct consequence of the phase-matching conditions used. However, we can make Eqs. (5) autonomous by substituting  $\mathcal{F}(\varphi, t) = F(\varphi, t) \exp(i\varphi/2)$ . Setting for uniformity  $\mathcal{S}(\varphi, t) = S(\varphi, t)$ , we arrive at the following autonomous generic set of nonlinear equations [19]:

$$\begin{aligned} \left( i\partial_t + i\frac{v_1}{R} \partial_\varphi + \frac{v'_1}{2R^2} \partial_\varphi^2 - \Delta_1 + i\gamma_1 \right) F &= 2\mu S F^* \\ \left( i\partial_t + i\frac{v_2}{R} \partial_\varphi + \frac{v'_1}{2R^2} \partial_\varphi^2 - \Delta_2 + i\gamma_2 \right) S &= \mu F^2 + ih \end{aligned} \quad (6)$$

for  $2\pi$ -periodic SH amplitude  $S$  and  $2\pi$ -antiperiodic FH amplitude  $F$ . In this set, the detunings  $\Delta_{1,2}$  are given by the expressions  $\Delta_1 = (\Delta_p + \Delta_q - v'_1/4R^2)/2$  and  $\Delta_2 = \Delta_p$ , where, as earlier,  $\Delta_p = \omega_{m_2^0} - \omega_p$  and  $\Delta_q = \omega_{m_1^0} + \omega_{m_1^0 + 1} - \omega_{m_2^0}$  are the pump and quasi-phase-match detunings. By setting  $\Delta_p = 0$  and varying  $\Delta_q$ , we can always achieve the case  $\Delta_{1,2} = 0$  relevant to our main results. Note that setting  $\Delta_p = \Delta_q = 0$  does not turn the detuning  $\Delta_1$  exactly to zero. However, the remnant detuning  $-v'_1/8R^2$  is typically negligible as compared to the FH line width  $2\gamma_1$ .

Setting  $\Delta_{1,2} = 0$  and  $\gamma_1 = \gamma_2 = \gamma$  in Eqs. (6), transferring to the coordinate frame moving with velocity  $v_1$  and to the normalized FH and SH amplitudes  $f = (\mu/\gamma)(2i)^{1/2} F$  and  $s = (2\mu/\gamma) S$ , and using the expansions

$$f(\varphi, t) = \sum_{j_1} f_{j_1}(t) e^{ij_1 \varphi}, \quad s(\varphi, t) = \sum_{j_2} s_{j_2}(t) e^{ij_2 \varphi} \quad (7)$$

with  $j_1 = \pm 1/2, \pm 3/2, \dots$  and  $j_2 = 0, \pm 1, \pm 2, \dots$ , we obtain a set of coupled ordinary differential equations for harmonics  $f_{j_1}$  and  $s_{j_2}$ :

$$\begin{aligned} \left( \frac{1}{\gamma} \frac{d}{dt} + i\beta_1 j_1^2 + 1 \right) f_{j_1} &= \sum_{j'_1} f_{j'_1}^* s_{j_1 + j'_1} \\ \left( \frac{1}{\gamma} \frac{d}{dt} - i\alpha j_2 + i\beta_2 j_2^2 + 1 \right) s_{j_2} &= \eta \delta_{j_2} - \sum_{j'_1} f_{j'_1} f_{j_2 - j'_1}. \end{aligned} \quad (8)$$

Here  $\alpha = v_{12}/\gamma R$ ,  $\beta_{1,2} = v'_{1,2}/2\gamma R^2$ , and  $\eta = 2\mu h/\gamma^2$  are dimensionless parameters. The product  $\gamma t$  can be treated as dimensionless time. Set (8) has to be solved with certain initial conditions for  $f_{j_1}$  and  $s_{j_2}$ . Achievement of a steady state corresponding to movement of the FH and SH envelopes  $f(\varphi, t)$  and  $s(\varphi, t)$  with a common velocity  $v_0 \neq v_1$  means that the steady-state amplitudes oscillate harmonically in time as  $\exp(-ijv_{01}t/R)$ .

### III. ESTABLISHMENT OF STEADY STATES: THE QUASI-ADIABATIC PROCEDURE

Here we exhibit representative data of numerical calculations relevant to transient processes and achievement of antiperiodic steady states for the FH and SF envelopes. Our quasi-adiabatic calculation procedure was organized as follows: The ordinary differential equations for 512 coupled FH and SH harmonics were solved in the time domain for different values of the walk-off parameter  $\alpha$ . The pump strength parameter  $\eta$  was increased stepwise from  $\eta_1 = 1.01$  to 30. For each discrete value  $\eta_s$  with  $s = 1, 2, \dots$ , we calculated velocity  $v_0(\eta_s)$  and the discrepancy parameter  $\varepsilon(t)$ , as defined in the main text, and made sure that it is saturated by  $t = t_s$  on an extremely low level ( $\varepsilon \sim 10^{-14} - 10^{-15}$ ). The values of the complex amplitudes  $F_{j_1}$  and  $S_{j_2}$  achieved by time  $t_s$  were used as initial conditions for a new

calculation run with  $\eta_{s+1} > \eta_s$ . This quasi-adiabatic iteration procedure was repeated until the maximum value  $\eta = 30$  was achieved. For the first calculation step, relevant to  $\eta_1 = 1.01$ , we started from a weak random noise,  $|f_{j_1}|^2, |s_{j_2}|^2 \lesssim 10^{-10}$  for  $j_2 \neq 0$  and  $s_0 = \eta_1$ . After reaching  $\eta_{\max} = 30$ , we repeated the quasi-adiabatic procedure by decreasing  $\eta$  and made sure that the same steady states were passed in reverse order.

Figure 2 shows representative examples of temporal evolution of the FH discrepancy parameter  $\varepsilon(t, \tau)$  for the time shift  $\tau = 1/\gamma$ . The first and second rows correspond to the walk-off parameter  $\alpha = 1$  and 0.1. The chosen 17

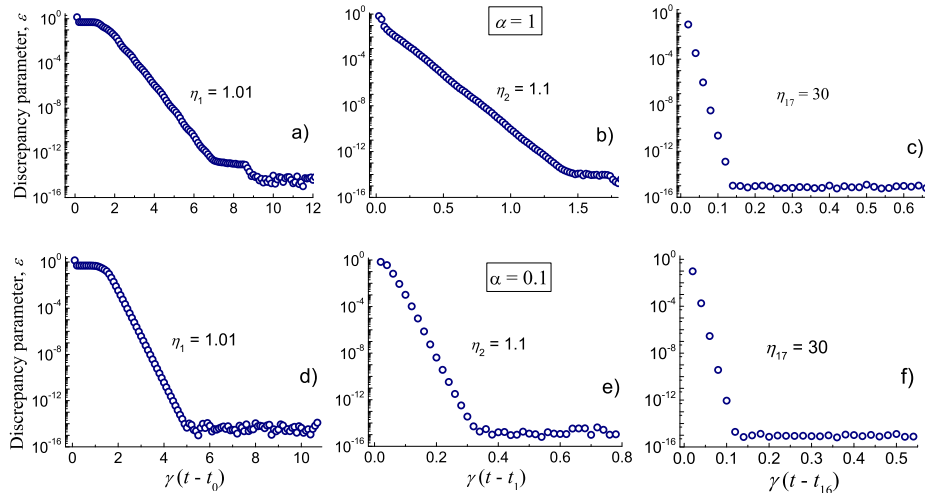


FIG. 2: Six representative evolution runs for the discrepancy parameter  $\varepsilon(t, \tau)$  at  $\gamma\tau = 1$ ; the time step is  $0.02\gamma^{-1}$ . The first and second rows correspond to  $\alpha = 1$  and 0.1, respectively. The evolutions relevant to a) and d) start at  $t_0$  from noise and end up at  $t_1$ . 512 harmonics are taken into account and the model parameters used in the simulations are:  $\gamma = 10^7 \text{ s}^{-1}$ ,  $\beta_1 = 0.02$ , and  $\beta_2 = -0.01$ .

values  $\eta_s$  are 1.01, 1.1, 1.3, 2., 2.5, 3, 3.5, 4, 5, 7, 10, 12, 15, 18, 20, 25, and 30. Subfigures a), b), c) and also d), e), f) exhibit evolution of  $\varepsilon$  for  $\eta_1$ ,  $\eta_2$ , and  $\eta_{17}$ . The most general feature this evolution is always the same: It is an almost exponential decrease of  $\varepsilon$  from initial values of the order of 1 to extremely low values  $10^{-14} - 10^{-15}$  caused by the numerical noise. Quantitative details of this evolution are also important. The longest evolution, subfigures a) and d), starts from modal noise. It takes  $\sim (5 - 7)\gamma^{-1}$  for the harmonics to grow exponentially and reach the saturation. The corresponding evolution time can be identified with the rise time of near-threshold optical parametric oscillation in microresonators. The further evolution runs, which start from regular distributions of the FH and SH harmonics achieved during the previous runs, occur substantially faster. Our choice of 17 steps of evolution to reach the soliton states with  $\eta = 30$  is largely arbitrary. In many cases, especially for  $\alpha \gtrsim 1$ , the same final state can be achieved even in one step. Variations of the time shift  $\tau$  give no effect on the data of Fig. 2. The temporal evolution of the SH discrepancy parameter behaves in a similar manner.

Anyhow, the numerical simulations evidence that our coherent antiperiodic soliton states, represented by Figs. 4-6 of the main text, are very robust. Not too abrupt turning the pump power on, with the pump rise time  $t_p$  exceeding  $10\gamma^{-1}$ , ensures achievement of these comb states. This restriction, relevant actually to  $t_p \gtrsim 1 \mu\text{s}$ , is very soft.

- 
- [1] R. W. Boyd, *Nonlinear Optics*, Academic Press (2008).
  - [2] T. Beckmann, et al., *Highly tunable low-threshold optical parametric oscillation in radially poled whispering gallery resonators*, Phys. Rev. Lett. **106**, 143903 (2011).
  - [3] I. Breunig, *Threewave mixing in whispering gallery resonators*, Laser and Photonics Review, **10**, 569 (2016).
  - [4] D. N. Nikogosyan, *Nonlinear Optical Crystals: A Complete Survey*, (Springer, 2005).
  - [5] M. Mohageg et al., *Calligraphic poling of lithium niobate*, Opt. Express **13**, 3408-3419 (2005)
  - [6] V. S. Ilchenko, A. A. Savchenkov, A. B. Matsko, and L. Maleki, *Nonlinear optics and crystalline whispering gallery mode cavities*, Phys. Rev. Lett. **92**, 43903 (2004).
  - [7] D. Strekalov, Ch. Marquardt, A. Matsko, H. Schwefel, and G. Leuchs, *Nonlinear and quantum optics with whispering gallery resonators*, J. Opt. **18**, 123002 (2016).
  - [8] S. Meisenheimer, J. Fürst, Ch. Werner, T. Beckmann, K. Buse, and I. Breunig, *Broadband infrared spectroscopy using optical parametric oscillation in a radially-poled whispering gallery resonator*, Opt. Express. **23**, 24042 (2015).

- [9] R. Wolf, Y. Jia, S. Bonaus, Ch. Werner, S. Herr, I. Breunig, K. Buse, and H. Zappe, *Quasi-phase-matched nonlinear optical frequency conversion in on-chip whispering galleries*, *Optica* **5**, 872 (2018).
- [10] J. Lu, J. B. Surya, X. Liu, A. W. Bruch, Z. Gong, Y. Xu, and H. X. Tang, *Periodically poled thin-film lithium niobate microring resonators with a second-harmonic generation efficiency of 250000 %/W* *Optica* **6**, 1455 (2019).
- [11] V. S. Ilchenko and A. B. Matsko, *Optical resonators with whispering-gallery modes, Part I: Basics*, *IEEE J. Quantum Electron.* **12**, 15-32 (2006).
- [12] B. Sturman and I. Breunig, *Generic description of second-order nonlinear phenomena in whispering-gallery resonators*, *J. Opt. Soc. Am. B* **28**, 2465-2471 (2011).
- [13] J. U. Furst et al., *Naturally phase-matched second-harmonic generation in a whispering-gallery-mode resonator*, *Phys. Rev. Lett.* **104**, 153901 (2010).
- [14] V. E. Zakharov and E. A. Kuznetsov, *Hamiltonian formalism for nonlinear waves*, *Physics-Uspekhi*, **40**, 1087 (1997).
- [15] T. Herr et al., *Temporal solitons in optical microresonators*, *Nature Photonics* **8**, 145-152 (2014).
- [16] T. J. Kippenberg, A. L. Gaeta, M. Lipson, and M. L. Gorodetsky, *Dissipative Kerr solitons in optical microresonators*, *Science* **361**, 567-572 (2018).
- [17] T. Hansson, P. Parra-Rivas, M. Bernard, F. Leo, L. Gelens, and S. Wabnitz, *Quadratic soliton combs in doubly resonant second-harmonic generation*, *Opt. Lett.* **43**, 6033-6036 (2018).
- [18] A. Villois and D. Skryabin, *Soliton and quasi-soliton frequency combs due to second harmonic generation in microresonators*, *Opt. Express* **27**, 7098-7107 (2019).
- [19] E. Podivilov, S. Smirnov, I. Breunig, and B. Sturman, *Nonlinear solutions for  $\chi^{(2)}$  frequency combs in optical microresonators*, Submitted (arXaiv 1910.03397).